Acta Cryst. (1993). D**49**, 389–402

Bovine Seminal Ribonuclease: Structure at 1.9 Å Resolution

BY LELIO MAZZARELLA

Dipartimento di Chimica, Università Federico II, *via Mezzocannone* 4, *I*-80134 *Napoli, Italy, and CEINGE, Biotecnologie Avanzate, Napoli, Italy*

AND SANTE CAPASSO, DOMENICO DEMASI, GUIDO DI LORENZO, CARLO ANDREA MATTIA AND ADRIANA ZAGARI

Dipartimento di Chimica, Università Federico II, *via Mezzocannone* 4, *I*-80134 *Napoli, Italy*

(*Received* 3 *August* 1992; *accepted* 5 *April* 1993)

Abstract

The crystal structure of bovine seminal ribonuclease, a homodimeric enzyme closely related to pancreatic ribonuclease, has been refined at a nominal resolution of 1.9 Å employing data collected on an electronic area detector. The final model consists of two chains containing 1990 non-H atoms, seven sulfate anions and 113 water molecules per asymmetric unit. The unit-cell parameters are $a = 36.5$ (1), $b = 66.7$ (1) and $c = 107.5$ (2) Å, space group $P22_12_1$. The R factor is 0.177 for 16 492 reflections in the resolution range 6.0–1.9 Å and the deviations from ideal values of bond lengths and bond angles are 0.020 Å and 3.7°, respectively. The molecule is formed by two pancreatic like chains, which have their N-terminal segments interchanged so that each active site is formed by residues from both subunits. The two chains are related by a non-crystallographic twofold symmetry and are covalently linked by two consecutive disulfide bridges, which form an unusual sixteen-membered ring across the dimer interface. The deviations from the molecular symmetry, the hydration shell and the sulfate-binding sites are also discussed in relation to the known structure of the pancreatic enzyme.

Introduction

Bovine seminal ribonuclease (BS-RNase) is a dimeric pyrimidine-preferring endoribonuclease isolated from bovine seminal plasma (D'Alessio, Di Donato, Parente & Piccoli, 1991, and references therein). It hydrolyzes the 3′,5′ phosphodiester bond *via* cyclic 2′,3′ intermediates, with a mechanism of action very similar to that of pancreatic ribonuclease A (RNase A) (Blackburn & Moore, 1982). However, the seminal enzyme can hydrolyze double-stranded RNA and gives non-hyperbolic saturation curves for the cyclic substrates of the second rate-limiting step of the reaction (Piccoli, Di Donato & D'Alessio, 1988). The two subunits have the same amino-acid sequence and are linked by two consecutive interchain disulfide bridges (Di Donato & D'Alessio, 1973). There is a pronounced homology between BS-RNase and RNase A: in particular, all residues important for the activity of the pancreatic enzyme and the eight half-cystines forming the intrachain disulfide bridges are preserved in the seminal enzyme.

The three-dimensional structure of BS-RNase has been determined previously by X-ray crystallography at 2.5 Å resolution (Capasso, Giordano, Mattia, Mazzarella & Zagari, 1983; Mazzarella, Mattia, Capasso & Di Lorenzo, 1987). Although each subunit closely resembled RNase A (Wlodawer & Sjölin, 1983; Borkakoti, Moss & Palmer, 1983; Wlodawer, 1985), the quaternary structure revealed that the N-terminal segments of the two chains had interchanged with respect to the pancreatic model, so that residues important for catalysis in each active site belonged to different subunits. These results prompted D'Alessio and coworkers to perform several experiments in solution from which they concluded that BS-RNase exists as two distinct conformational isomers: a major isomer characterized by the interchange of the N-terminal segments and a minor isomer in which this phenomenon does not occur (Piccoli *et al.*, 1992). As our proposed structure was crucially dependent on the modelling of the short peptide 16–22, not particularly well defined in the electron-density map, we collected a new set of data extending to 1.9 Å resolution using an electronic area detector, to replace the diffractometer data obtained at lower resolution from several crystals. The new data set was used to confirm the previous interpretation of the structure for the peptide 16–22 and to derive a more accurate model of the protein. We now report the results of these analyses including the solvent structure and location of the sulfate anions.

ISSN 0907-4449 ©1993

Experimental

Notation

The IUPAC–IUB Commission on Biochemical Nomenclature (1970) conventions are generally used. M1 is the model based on the diffractometer data. The two chemically equivalent subunits of BS-RNase, related by non-crystallographic twofold symmetry, are called *S*1 and *S*2, respectively; for each chain, fragments 1–15 and 23–124 are called *T* (tail) and *B* (body), respectively, fragment 16–22 is the hinge peptide. Following the classification given by Wlodawer (1985) for RNase A, the three helical regions in each subunit of BS-RNase span residues 3–13, 24–34, 50–60, and are denoted *H*1, *H*2 and *H*3, respectively.

Residues are indicated by the conventional three-letter or one-letter code followed by the sequence number 1 to 124; in the figures and wherever it is necessary for clarity, the residue number of *S*2 is augmented by 500. Sul and Wat (S and W in figures) stand for the sulfate anions (sequence number 125 to 128) and water molecules (sequence number greater than 130), respectively, and were assigned to *S*1 or *S*2 according to their strongest interactions.

The molecule has composite active sites, that is each active site is formed by residues belonging to different chains. As the molecular twofold axis is a non-crystallographic symmetry element, the two sites are distinguishable: *AS*1 is the site formed by His12 of *S*2 (His512) and His119 of *S*1, *AS*2 is the site formed by the complementary residues. The side chain of His119 adopts two conformations: *t* is the conformation most frequently found in RNase A ($\chi^1 \simeq 180°$), g^- is the alternative conformation ($\chi^1 \simeq -60°$).

5RSA, 3RN3 and 1SRN are the codes of Brookhaven Protein Data Bank files which contain the coordinates of RNase A (Wlodawer & Sjölin, 1983), RNase A (Howlin, Moss & Harris, 1989) and a semisynthetic ribonuclease (Martin, Doscher & Brian, 1987), respectively.*

Crystals and X-ray data

Crystals of BS-RNase were obtained by batch and vapour-phase equilibration methods at room temperature. In both cases, large crystals (up to 0.8 × 0.4 × 0.2 mm) were grown in three or four weeks from a solution of the enzyme at concentration in the range 15–20 mg ml^{-1}, ammonium sulfate at 80% saturation, ammonium phosphate 0.1 m*M* and acetate buffer 10 m*M* (pH ~ 5.1). The crystals are orthorhombic with unit-cell parameters $a = 36.5$ (1), $b = 66.7$ (1), $c = 107.5$ (2) Å, space group $P22_12_1$, $Z = 4$. X-ray diffraction data were collected with a Siemens imaging proportional counter (IPC), mounted on a Supper oscillation camera controlled by a PCS computer. Cu $K\alpha$ radiation was provided by a Rigaku RU-200 rotating anode operating at 50 kV, 100 mA. The detector was positioned at a distance of 10 cm from the crystal and at angles of 0 and 25°. In the latter case, two positions of the φ circle were chosen ($\Delta\varphi = 90°$). For each orientation of the crystal, 400 data frames were collected covering, on the whole, 100° rotation of the ω circle. In a single frame, reflections resulting from a 0.25° oscillation of the crystal were recorded in 180 s. All data were collected on two crystals. Crystal orientation and integrated intensities were calculated with the *XENGEN* program system (Howard *et al.*, 1987). After scaling, 59 869 recorded reflections were merged to give 18 916 unique reflections (~ 90% of the expected number of reflections to 1.9 Å resolution) and 17 217 having $I > 3\sigma(I)$. The merging R factor based on intensity, $R = \sum_h\sum_i|I_{hi} - \langle I_h\rangle|/\sum_h\sum_i\langle I_h\rangle$ (I_{hi} is the intensity of the ith measurement of a reflection, $\langle I_h\rangle$ the mean intensity for that reflection and the summations are over all the measurements), was 0.067 for all data to 1.9 Å resolution. The Wilson plot (Wilson, 1949) of the data (Fig. 1) shows the expected deviations from linearity for a protein crystal in the low-resolution range. A better fit to the theoretical straight line was obtained, *a posteriori*, by estimating the average intensity in each shell of $(\sin\theta/\lambda)^2$ from the model using a zero thermal factor. The overall temperature factor from the plot, 9.2 Å^2, is significantly lower than the value obtained from the diffractometer data. Once this difference had been allowed for and after scaling, the R factor between the intensities of the two data sets was 0.12.

Refinement

The new set of data was first used to check the structure previously proposed for the hinge peptide 16–22 of the two chains. In order to minimize bias from the previous model (Mazzarella *et al.*, 1987), the M1 coordinates were refined by means of the simulated annealing (SA) procedure (Brünger, Kuriyan & Karplus, 1987) with the program *X-PLOR* in the resolution range 6.0–1.9 Å, excluding from the model the two hinge peptides. Water molecules were also excluded from the refinement and border residues of the omitted peptides (Ser15, Ser23, Ser515 and Ser523) were harmonically restrained to the starting positions. The w_a weight,

* Atomic coordinates and structure factors have been deposited with the Protein Data Bank, Brookhaven National Laboratory (Reference: 1BSR, R1BSRSF). Free copies may be obtained through The Technical Editor, International Union of Crystallography, 5 Abbey Square, Chester CH1 2HU, England (Supplementary Publication No. SUP 37083). A list of deposited data is given at the end of this issue.

which relates the effective X-ray energy to the empirical potential energy of the protein, was estimated at 120 000 kJ mol^{-1}, following the procedure suggested by Brünger, Karplus & Petsko (1989). The weight applied to each X-ray observation was $w_{hkl} = 1/\sigma^2$, where $\sigma = 27$–80 $(\sin\theta/\lambda - 0.01667)$. The molecular dynamics simulation was started at $T = 1200$ K with a cooling rate of 25 K every 25 fs and was preceded and followed by 80 cycles of conjugate-gradient X-ray energy-restrained minimization. The resulting coordinates gave an R factor $(\sum||F_o| - |F_c||/\sum|F_o|)$ of 0.22 and were used to calculate an omit $(|F_o| - |F_c|)\exp(i\alpha_c)$ Fourier map (see Fig. 8*a*), which fully confirmed the previous model, except for the orientation of the peptide unit 17–18 which was flipped.

Successively, the complete M1 model was refined by the energy-restrained minimization procedure of *X-PLOR* using 16 492 reflections with $I > 3\sigma(I)$. w_a and w_{hkl} were set to the values used in the SA run. In the course of the refinement only a few manual modifications of the structure were made, using the interactive computer program *FRODO* (Jones, 1978) running on an Evans & Sutherland PS390 graphics system. Side chains of His119 of *S*1 and Asn71 of *S*2 were modelled in two conformations and refined using group-occupancy factors the sum of which was unity for the two alternative positions. For a few cycles a group-occupancy factor was also refined for each of the seven sulfate anions, but only those of the two groups located in the active sites between the two histidine residues refined to a value slightly less than one; therefore, full occupancy was used for all of them. On a few occasions, 30 cycles of restrained

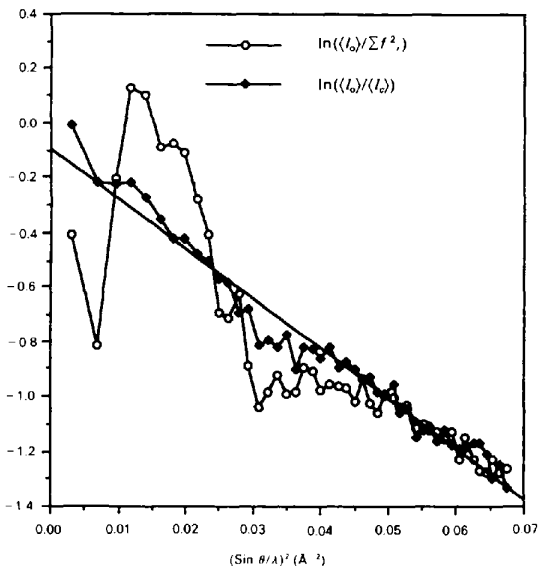

Fig. 1. The Wilson plot for the data extending to 1.9 Å resolution.

Table 1. *Final R factors*

Resolution limits (Å)	∞ 1.9	∞ 6.0	6.0–1.9
Number of reflections [$I > 3\sigma(I)$]	17217	725	16492
Final R factors with the contribution of			
All non-H atoms	0.233	0.518	0.186
All atoms	0.240	0.555	0.183
All atoms plus disordered solvent	0.184	0.287	0.177

isotropic temperature-factor refinement were performed until convergence was achieved. Target values for the difference in thermal parameters between main-chain atoms separated by one or two bonds were 1.0 and 1.5 Å^2, respectively, while the target values for side-chain atoms were 2.0 and 2.5 Å^2.

At convergence, a selected set of water molecules was removed from the atom list and the structure was subjected to a few cycles of refinement. A difference Fourier map was then calculated in the region of interest and all peaks above 0.3 e Å^{-3} were examined. This procedure was repeated to cover all the asymmetric unit. Water molecules were located under the condition that the peak had an approximate spherical shape and that it was placed within hydrogen-bonding distances from protein atoms or another water molecule. The solvent O atoms were then allowed to refine for several cycles. The occupancy factor of the water molecules was set to one and the sites which acquired a B factor greater than 60 Å^2 during the refinement were rejected.

At this stage H atoms were introduced in the refinement at the calculated positions with the B factor of the parent atoms and, finally, the contribution of the disordered solvent in the crystal was estimated and added to the calculated structure factors, while 725 lower order reflections ($d > 6.0$ Å) were also added to the calculations.

Refinement converged to an R value of 0.177 for 16 492 reflections in the range 6.0–1.9 Å with $I > 3\sigma(I)$. At convergence the highest peak in the difference Fourier map had a value of 0.70 e Å^{-3}: this was located on the crystallographic diad axis, more than 4 Å from any determined atomic site. With this exception, no peak had an absolute value greater than 0.35 e Å^{-3}. The final crystallographic R factors are reported in Table 1. Throughout the refinement, restraints related to the local twofold symmetry were not applied.

Disordered solvent

To calculate the contribution of the disordered solvent to the diffraction pattern, the unit cell was divided in a grid of about 0.5 × 0.5 × 0.5 Å^3 and for each grid point the electron density ρ, contributed to by all the protein atoms and the ordered solvent molecules, was calculated using for each atom a two-Gaussian function which includes the isotropic

thermal factor as a parameter (Agarwal, 1978). All the grid points with an associated $\rho < \rho_{min}$ were considered occupied by the solvent and were assigned a constant electron density calculated from the known composition of the solvent (~ 0.4 e Å^{-3}). The value of $\rho_{min} = 0.015$ e Å^{-3} was chosen to give a value of 0.46 for the fraction of the grid points assigned to the bound and disordered solvent, in agreement with an earlier estimate of the fractional volume of the solvent in these crystals (Capasso, Giordano, Mazzarella & Ripamonti, 1972). The contribution F_{dis} of the disordered solvent density was calculated for each reflection and added to the 'ordered' contribution F_{or} to give $F_c = F_{or} + KF_{dis}\exp(-B\sin^2\theta/\lambda^2)$. The values $K = 1.14$ and $B = 67.7$ Å^2 were obtained by a least-squares fit of F_c's to the experimental data.

Results

A view of the C$^\alpha$-atom model of the molecule is shown in Fig. 2. The two chains *S*1 and *S*2 are related by a local twofold axis approximately parallel to *c* (vertical axis in Fig. 2). The molecular symmetry is closely fulfilled by most atoms of the molecule, though large deviations are observed for the hinge peptide and for the exposed loop 65–72 (see also Figs. 9 and 10). With the exclusion of these areas, the r.m.s. deviation of main-chain torsion angles φ and ψ between *S*1 and *S*2 is about 7°, a value which is remarkably low considering that restraints related to the local twofold symmetry were not applied in the refinement. Thermal parameters, shown in Fig. 3 for main-chain and side-chain atoms, also present a high degree of correlation between the two subunits as evidenced by the plot of Fig. 4 for backbone atoms. The average *B* value for the non-H protein atoms is 11.9 Å^2 (10.2 and 13.9 Å^2 for backbone and side chains, respectively), slightly higher than the value of 9.2 Å^2 obtained from Wilson statistics.

Accuracy of the model

Compared to the standard level of the structures stored in the Protein Data Bank, the bond parameters in the final model are satisfactory. On average, bond lengths and valence angles differ 0.020 Å and 3.7°, respectively, from the corresponding ideal values set by *X-PLOR*, and only 0.7% of the total number deviates more than 3σ. For backbone atoms, the r.m.s. deviation of bond lengths and valence angles from their mean values is 0.016 Å and 2.6°, respectively. In Table 2 the mean values, e.s.d.'s and the minimum and maximum values for representative valence angles are compared with those derived from a statistical analysis of the crystal structures of a large number of small non-Pro peptides (Ashida, Tsunogae, Tanaka & Yamane, 1987). For the bond angles $\tau_{C'}$ and τ_N the two distributions agree reasonably well, whereas for τ_{C^α} the values of our model show a greater spread about the mean. This is probably correlated to the distribution of the peptide dihedral angle ω, which is much sharper in the protein model, suggesting that the parameters restraining the planarity of the peptide unit are relatively overestimated in the *X-PLOR* force field. For the 23 aromatic planar groups the r.m.s. deviation from planarity is 0.01 Å.

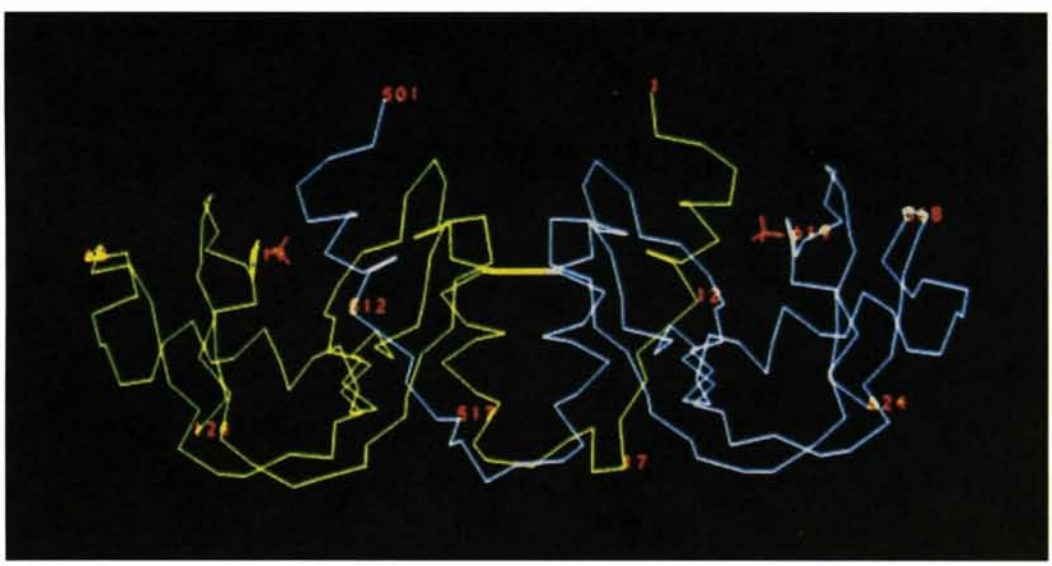

Fig. 2. C$^\alpha$-atom drawing of BS-RNase: different colours are used for the two chains. The two interchain disulfides (in yellow) are superimposed. The molecular diad axis is vertical.

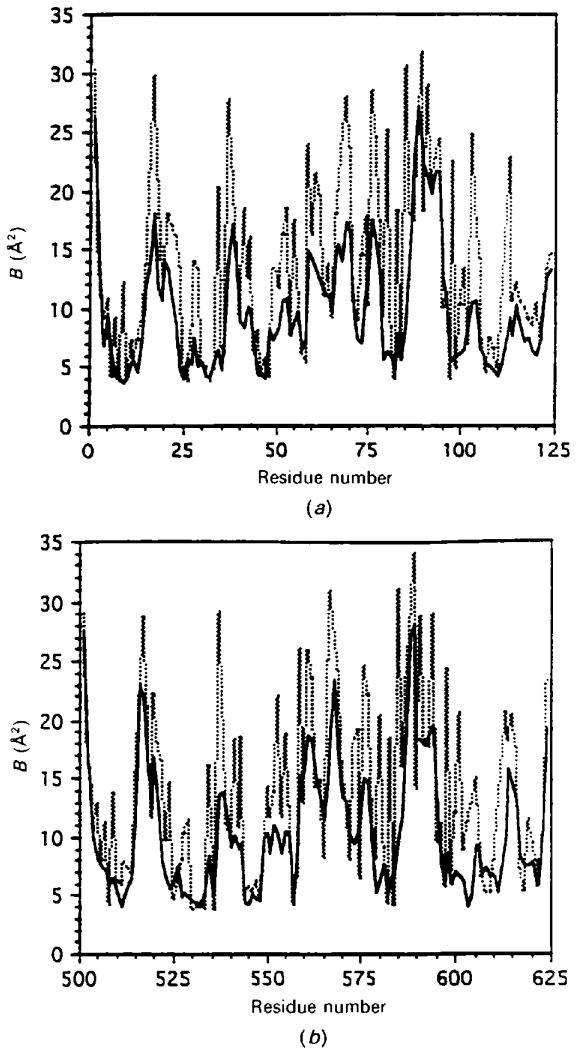

Fig. 3. Variation in the temperature factor B per residue along the $S1$ (*a*) and $S2$ (*b*) subunits. Full and dotted lines refer to backbone and side-chain atoms, respectively.

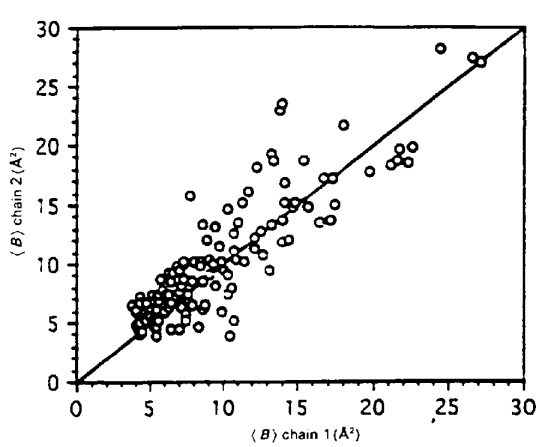

Fig. 4. Correlation of the thermal factors between $S1$ and $S2$ residues. $\langle B \rangle$ is the r.m.s. thermal factor per residue of main-chain atoms.

Table 2. *Mean, spread, minimum and maximum values* (°) *of the distribution for selected bond angles and the dihedral angle* ω

	Small peptides*				BS-RNase			
	Mean	σ	Min.	Max.	Mean	σ	Min.	Max.
τ_C	116.2	2.1	110	125	116.3	2.1	111	123
τ_N	121.5	1.8	115	126	120.8	1.9	116	126
$\tau_{C\alpha}$	110.9	2.8	103	117	110.1	4.6	99	125
ω	178.9	6.4	157	201	179.7	0.8	177	182

* Values for any residue X = non-Pro in X non-Pro sequences (Ashida *et al.*, 1987).

An upper limit of the mean positional error, as estimated from the Luzzati (1952) plot shown in Fig. 5, is in the range 0.20–0.25 Å. A somewhat smaller value (~0.1 Å) is suggested by the r.m.s. deviation between the corresponding main-chain atoms, resulting from the superposition of the two subunits (see below).

Fig. 6 shows the real-space reliability factor $R_{rs}(i) = \sum|\rho_o(i) - \rho_c(i)|/\sum|\rho_o(i) + \rho_c(i)|$ (Jones, Zou, Cowan & Kjeldgaard, 1991), computed as a function of residue number. ρ_o and ρ_c are the observed ($2F_o - F_c$) and calculated density maps of the final model. The summation was extended over all grid points with $\rho > 0.015$ e Å^{-3} of a model density (see *Disordered solvent*) calculated with the contribution of all atoms (dotted line) and N, C^α, C, O, C^β atoms (full line) from two equivalent residues of $S1$ and $S2$. In each case, the grid points included in the summation correspond to more than 99% of the total electrons of the selected residues. The R_{rs} factor is fairly constant all over the structure and documents the quality of the local fit of the model to the observed density. The largest discrepancies are found for Lys1, Gly88 and Ser89; these residues correspond to ill defined regions of the map and also present the largest thermal parameters for main-chain atoms (Fig. 3). In addition, Lys34, Lys566, Asn567, and Gln37, Lys76, Arg85, Lys91 and Lys98 of both chains also have ill defined density at the side-chain level.

The Ramachandran plot (Ramakrishnan & Ramachandran, 1965) of the main-chain torsion angles φ

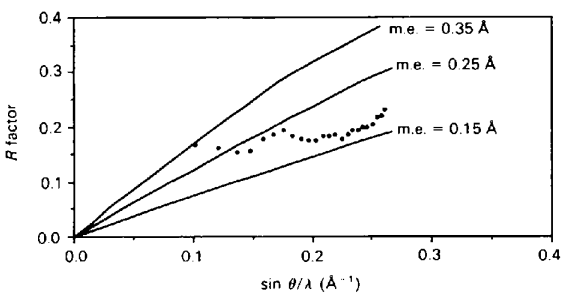

Fig. 5. Plot of the R factor as a function of the resolution after Luzzati (1952). m.e. is the mean error of the atomic coordinates.

and ψ is shown in Fig. 7. The few points outside the sterically allowed regions are glycine residues (represented by open squares) with the exception of Gln60, which is placed at the end of the helix *H*3 and adopts similar conformation in RNase A. Three non-glycine residues Lys34, Lys534 and Asn571 fall in the left-handed α-helical region ($L\alpha$). In both chains, residue 34 is at the C-terminal end of the *H*2 helix, which presents a π-type hydrogen bond between Met30 and Met35 and a 3_{10} hydrogen bond between Cys31 and Lys34. In this type of distortion at the C-terminal end of an α-helix, the donor of the 4→1 bond has the $L\alpha$ conformation. In RNase A residue 34 is Asn, which has a strong preference for this conformation; replacement of Asn for Lys in the seminal enzyme does not alter the local structure of the chain at all.

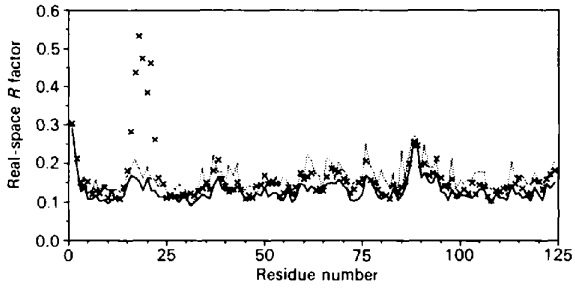

Fig. 6. The main-chain (full line) and all atoms (dotted line) real-space R_{rs} factor as function of residue number. Each value of R_{rs} includes contributions from corresponding residues of *S*1 and *S*2. Crosses represent main-chain values of R_{rs} calculated from the BSA model (see text).

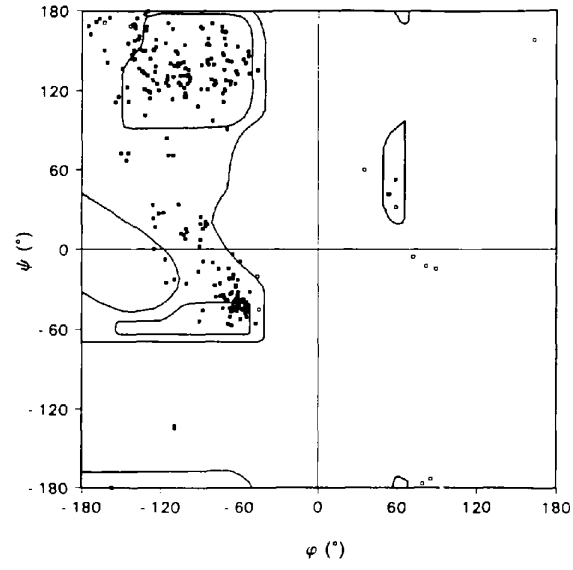

Fig. 7. Ramachandran plot of BS-RNase. Glycine residues are marked with open squares.

Except for Asn, the distribution of side-chain conformations is in fairly good agreement with the values reported by Ponder & Richards (1987). Out of 14 asparagine residues, six have the uncommon conformation with $\chi^1 \simeq 180$ and $\chi^2 \simeq 60°$. However, four out of the six residues are engaged in strong hydrogen bonds. Asn567, Arg585 and a few lysine residues, which assume an unfavourable conformation, are badly defined in the density map.

Hinge peptides

Fig. 8(*a*) shows a stereoview of the omit difference Fourier map calculated at the end of the simulated-annealing run performed with the exclusion of the two hinge peptides 16–22 (see *Refinement*). The map, seen approximately down the molecular twofold axis, was contoured at 2σ level, where σ is the r.m.s. deviation of the electron density in the unit cell. In spite of the bias introduced by refining a model which had no atoms in this region, the Fourier map is well defined and gives an unambiguous indication of the chain tracing, the final model of which is also shown as thick lines.

An alternative model of the hinge peptides was obtained by superimposing the structure of the *T*/*B* segments of RNase A on the *T*1/*B*2 and *T*2/*B*1 segments, respectively, of the seminal enzyme (see below). The hinge peptides of the dimer reconstructed with this procedure (BSA model) are shown in Fig. 8(*b*) as thin lines superimposed on BS-RNase model. In the BSA model, the two hinge peptides connect *T*1 to *B*2 and *T*2 to *B*1, respectively, and appear to be sterically compatible with the remaining part of the dimer. This model was extensively refined against the experimental data using the program *X-PLOR*. Throughout the refinement, the crystallographic *R* factor of BSA remained about 0.02 greater than the corresponding *R* value of the interchanged dimer. The R_{rs} factor of the refined BSA model, calculated as function of residue number is represented by crosses in Fig. 6 and clearly indicates that for the seminal enzyme the pancreatic conformation of the hinge peptide is incorrect.

Furthermore, the difference Fourier map, based on the final correct model, is featureless, supporting the conclusion that dimers with an alternative conformation of these peptides are not present at an appreciable level in our crystals. On the basis of the results obtained by Piccoli *et al.* (1992) showing the presence of both dimers in solution, we conclude that under the conditions used to grow crystals of BS-RNase only the most abundant conformational isomer is selected.

Deviations from the molecular twofold symmetry of the hinge peptide are determined mainly by the different conformations adopted by Gly16, Asn17,

Ser18 and Ser21. Pro19 in both subunits is *trans* and is part of a β-bend stabilized by a 4→1 hydrogen bond between the carbonyl group of Ser18 and the amide group of Ser21 (2.9 and 3.0 Å in *S*1 and *S*2, respectively). The Ser21 to Ser23 fragment forms one turn of a distorted 3_{10} helix, which bends at the level of Asn24 and proceeds with α-type 5→1 bonds as found in RNase A (*H*2 helix).

Loop 65–72

Large deviations from the twofold symmetry are observed for the exposed loop 65–72 (Figs. 9 and 10). In the crystal the *S*1 loop is in a close contact, across the local twofold axis, with the *S*2 loop of a molecule translated one unit cell along the *b* axis. In *S*1 the conformation of this peptide is close to the one found in RNase A and a similar conformation of *S*2 would cause a large interpenetration of the two peptides. This is avoided by a small tilt of the molecular twofold axis and a large conformational change of the *S*2 loop. With respect to *S*1, residues 67–71 of *S*2 are displaced more than 4 Å toward the inside of the chain, and lose the intraloop hydrogen bonds which stabilize the pancreatic folding.

It must be pointed out that in the region of the *S*2 loop the electron density is less well defined and this is probably a consequence of a heterogeneity of the chain. Indeed, it has been shown that BS-RNase deamidates selectively at Asn67 much faster than RNase A and the purified material is a mixture of fully amidated (β_2), mono-deamidated ($\alpha\beta$) and doubly deamidated (α_2) subforms, in the approximate ratio 6:3:1. Each deamidated subform is a mixture of *n*-aspartyl and iso-aspartyl derivatives with a strong preponderance of the last form (Di Donato & D'Alessio, 1981). In addition, during the crystallization step, the high ionic strength of the crystallization solution is likely to increase the relative concentration of the $\alpha\beta$ and α_2 subforms, although the pH of the solution at ~5.1 is not favourable to the deamidation reaction (Capasso, Mazzarella & Zagari, 1991). A chromatographic analysis of dissolved crystals indicated that the various subforms were also present in the crystals. On the basis of the crystal packing, of the large conformational change that occurs in the region of Asn67 and of the poorer quality of the electron-density map in the region of the *S*2 loop, it seems likely that the major contaminant, the $\alpha\beta$ iso-aspartyl derivative, may adopt a preferential orientation with respect to the local twofold axis, by placing the iso-aspartyl chain in the *S*2 position. No attempt was made to model the *S*2 chain as the iso-aspartyl derivative.

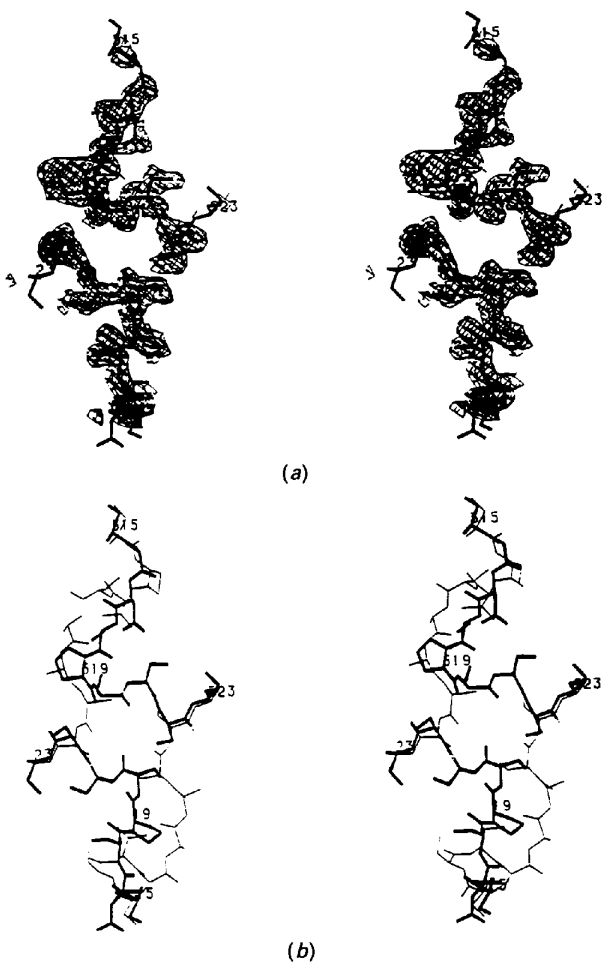

Fig. 8. (*a*) Stereo drawing of the electron density from an omit $(|F_o| - |F_c|)\exp(i\alpha_c)$ map (see text) in the region of the two hinge peptides 16–22, with the final model shown as thick lines. The map is contoured at the 2σ level. (*b*) Stereo drawing of the final model of the hinge peptides (thick lines). The RNase model of the peptide is shown as thin lines (see text).

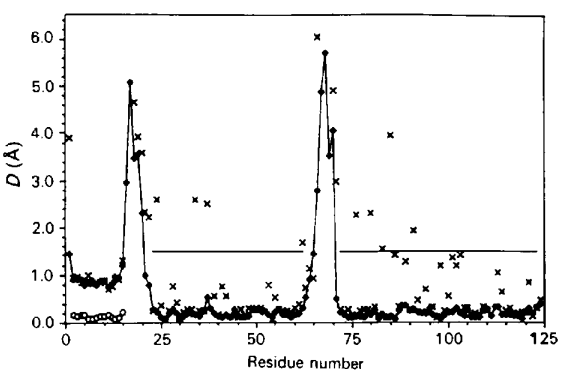

Fig. 9. Mean difference positons *D*, when superimposing *B*1 and *B*2 segments (horizontal lines span residues used for the superposition, see text): (◆) between main-chain atoms; (×) between side-chain atoms. (o) *D* between main-chain atoms of residues 2–15, when superimposing the segments *T*1 and *T*2.

Molecular symmetry

Because of the extensive interchain *T*/*B* interactions, the details of the symmetry operation which relates the two chains were analyzed for the *T* and *B* segments separately. In the first case, the backbone atoms of residues 2–15 and, in the second case, those of residues 23–62 and 72–123 were considered. The polar coordinates ψ and φ of the rotation axis (defined with respect to the z and x axes, respectively), the amount of the rotation χ about the axis, and the translational component τ along the rotation axis, are given in Table 3, together with the number of main-chain atoms used for the superposition. The last three columns give the r.m.s. deviation for the *B*, *T* and *T*/*B* segments. The r.m.s. deviations for the *B*2→*B*1 superposition as function of the residue number are also shown in Fig. 9. All these figures indicate the close similarity of the two chains and are comparable to the values obtained, for instance, for the two molecules in the asymmetric unit of two covalent nucleoside derivatives of RNase A (Nachman *et al.*, 1990).

The symmetry operation for both segments is a twofold rotation coupled to a small but significant translation τ parallel to the molecular axis. The values of τ for the *B*2→*B*1 and *T*2→*T*1 superpositions have approximately equal magnitude but opposite sign (differences in $|\tau|$ may not be meaningful in view of the much lower number of equivalences used for the *T*2→*T*1 superposition).

Table 3. *Analysis of the molecular symmetry*

n is the number of main-chain atoms used for the superposition. ψ and φ are the polar coordinates of the rotaton axis, defined with respect to the z and x axis, respectively, and χ is the amount of rotation about the axis. τ is the translational component along the axis. The r.m.s. displacement was calculated for the segments indicated by the column heading.

Structure superimposed	*n*	Transformation parameters ψ (°)	φ (°)	χ (°)	τ (Å)	R.m.s. deviation (Å) *B*	*T*	*TB*
*B*2→*B*1	368	1.7	−66.6	180.4	0.35	0.21	0.89	0.38
*T*2→*T*1	56	1.2	−86.5	180.7	−0.48	1.10	0.14	1.03
*B*2/*T*1→*B*1/*T*2	424	1.5	−68.5	180.4	0.41	0.22	0.25	0.22

Because of the particular relationship between the *T* and *B* domains in the dimer, the screw component of the molecular symmetry, though small, has an interesting consequence. This can be seen in Fig. 10, where *S*2 and *S*1 were superimposed using the transformation which gives the best *B*2→*B*1 superposition: the relative position of *T* is shifted ~0.8 Å along the rotation axis. This displacement forces the hinge peptides to adopt a different conformation in the two chains, as indeed was found. On the other hand, a superposition of *T*1/*B*2→*T*2/*B*1 (the last line in Table 3) gives an r.m.s. deviation for the *T*/*B* domain only slightly higher than the values calculated by superposing each segment separately. Therefore, in spite of *T*1 being covalently linked to *B*1, the domain *T*1/*B*2 (and *T*2/*B*1) behaves as a single structural unit, largely unaffected by the deviation of the molecule from the exact twofold symmetry, which, *vice versa*, influences the conformation of the hinge peptide. This result might have been expected in view

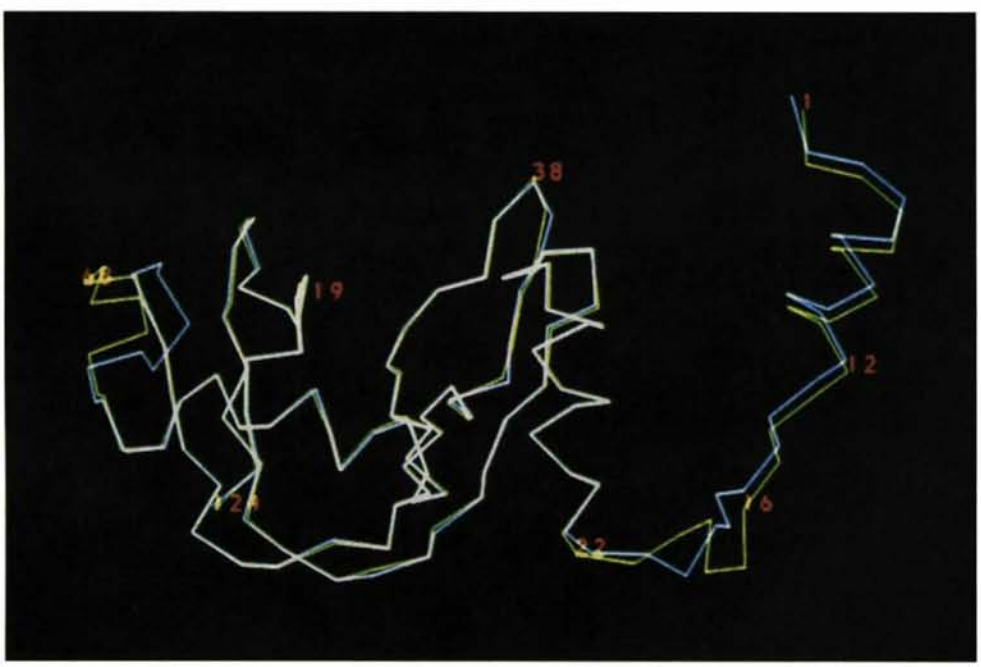

Fig. 10. C^{α}-atom drawing of superimposed chains. The superposition was obtained using the main-chain atoms of residues 23–62 and 72–123.

of the large *T1*/*B2* (*T2*/*B1*) contact region and the number of hydrogen bonds between the two segments (Table 4).

Disulfide bridges

The two chains are linked by two disulfide bonds (Fig. 2) connecting residues 31 and 32 of one chain to residues 32 and 31 of the other chain, respectively. The two consecutive interchain disulfide bonds form a sixteen-membered ring, which embodies two antiparallel peptide groups located at the C-terminal end of the two *H2* helices of the dimer.

The conformational parameters of all intrachain and interchain disulfide bridges are given in Table 5. Torsion angles for the two chains are remarkably similar; the only major difference is in the intraloop 65–72 bridge. The r.m.s. deviation is 4°, and a value only slightly higher (9°) is obtained when the intrachain disulfides are compared with those of RNase A. Six out of the eight intrachain disulfides belong to the left-handed spiral conformation and the remaining intrachain bridges have a right-handed hook conformation (Richardson, 1981). In the sixteen-membered rings formed by the interchain disulfides, the twofold symmetry is strictly fulfilled and the bridges are characterized by a χ^3 close to 90° and C^α—$C^{\alpha\prime}$ distances in the expected range. The combination of χ^1 and χ^2 values, however, gives rise to a conformation not commonly found in proteins, as are the constraints determined by the closure condition and the twofold symmetry of the ring embodying the two disulfides.

Comparison with RNase A

Coordinates of RNase A, taken from the file 5RSA (Wlodawer & Sjölin, 1983), were rotated and translated to give the best superposition with the structural unit *T2*/*B1* and *T1*/*B2* of the seminal enzyme. Using the backbone atoms of residues 2–15, 23–62 and 72–123, the r.m.s. deviation was 0.54 Å with either of the two subunits. Apart from the hinge peptide and the loop 65–72 of *S2*, the largest differences (1–2 Å) were observed for residues 37–38, 113–114 and 87–94. In the first case the difference is caused by the orientation of the peptide unit which differs by 180° in the two molecules. This is likely to be a genuine difference related to the change in the amino-acid sequence from Lys-Asp in RNase A to Gln-Gly in the seminal enzyme. Furthermore these residues are in contact with residues Gly611-Gly612 of a screw-related molecule and the carbonyl group of Gln37 is hydrogen bonded to the amide N atom of Gly612. Residues 87–94 form an exposed loop, which in BS-RNase is slightly bent with respect to RNase A in the same direction for both chains. When these segments were also excluded from the comparison, the r.m.s. deviation for the 332 equivalences is reduced to 0.36 Å for each chain.

This value clearly indicates the close similarity of the structural unit used to compare the two enzymes, although the segments *T* and *B* of the unit are connected by the hinge peptide in RNase A but bonded to *B* and *T* of the symmetry-related unit in the seminal enzyme. The similarity of interactions between the segments *T* and *B* is also clear from the list of the hydrogen bonds in Table 4. The difference in the interaction between Asp14 and His48 is probably related to the structural changes which occur in the hinge peptide.

*Active sites and the conformation of His*119

The conformation of the mobile His119 side chain has been extensively discussed in connection with the various refined structures of RNase A. Borkakoti *et al.* (1983) modelled the imidazolyl group in two alternative positions and they estimate a weight of 0.8 for the conformation *t* and 0.2 for the conformation g^- (Table 6). Wlodawer & Sjölin (1983) found the histidine in conformation *t*, and placed a water molecule in the alternative position. More recently, in the high-resolution structure of sulfate-free RNase A, several side chains were modelled in two alternative positions, but the authors found no indication on the electron-density map that might suggest the presence of the conformation g^- for His119 (Campbell & Petsko, 1987; Wlodawer, Svensson, Sjölin &

Table 4. *Hydrogen-bonding interactions* (Å) *between T and B segments*

Interactions mediated by the sulfate groups are not included.

T	*B*	*T1*/*B2**	*T2*/*B1**	*T*/*B*†
His12 O	Val47 N	2.70	2.82	2.82
Asp14 N	Val47 O	2.99	3.10	2.50
Arg10 $N^{\eta 2}$	Arg33 O	2.89	2.82	3.09
Arg10 O	Arg33 $N^{\eta 2}$	2.76	2.79	2.97
Gln11 O	Asn44 $N^{\delta 2}$	2.78	2.81	2.76
His12 $N^{\delta 1}$	Thr45 O	2.85	2.77	2.70
Met13 O	Arg33 $N^{\eta 1}$	2.85	2.96	2.75
Met13 O	Arg33 $N^{\eta 2}$	2.99	2.97	2.95
Asp14 O	His48 $N^{\delta 1}$	2.94	3.09	3.43
Ser15 O^γ	Glu49 O	2.69	2.79	2.62
Asp14 $O^{\delta 2}$	Tyr25 O^η	2.67	2.53	2.67
Ala4 O	Wat139 Val118 O	2.80/2.71	2.81/2.61	2.86/2.42
Ala5 O	Wat132 Pro117 O	3.30/2.92	3.25/2.80	2.74/2.91

* Seminal ribonuclease
† Coordinates of RNase A from the file 5RSA.

Table 5. *Torsion angles* (°) *and* C^α—$C^{\alpha\prime}$ *distances* (Å) *for disulfide bridges*

Values for *S2* are given in parentheses.

Cys—Cys′	χ^1	χ^2	χ^3	$\chi^{\prime 3}$	$\chi^{\prime 1}$	C^α—$C^{\alpha\prime}$
26—84	−72 (−77)	81 (−79)	−81 (−86)	−57 (−50)	−64 (−67)	5.6 (5.6)
40—95	−60 (−59)	−55 (−60)	−90 (−88)	−61 (−59)	−59 (−56)	5.7 (5.5)
58—110	−69 (−72)	54 (−53)	−88 (−90)	−107 (−109)	68 (−64)	5.7 (5.8)
65—72	52 (57)	−70 (−70)	114 (105)	87 (102)	−81 (−80)	5.3 (5.2)
31—532	169	−149	93	52	176	5.2
531—32	173	−150	89	55	173	5.2

Gilliland, 1988). On the other hand, in the crystal structure of a semisynthetic ribonuclease only the g^- conformation was found (Martin *et al.*, 1987).

Similar contrasting results have been obtained for the seminal enzyme. In *AS*1 there is clear evidence for the presence of the t and g^- conformations with the last conformation slightly more populated, whereas in *AS*2 only the g^- conformation is visible (see Fig. 11). The refined values of the side-chain torsion angles χ^1 and χ^2 for the conformation t and g^- of His119 are given in Table 6.

In the seminal enzyme the different behaviour of His119 and His619 can be related to the different structure of the loop 65–72. Fig. 12 shows a view of the two active sites side by side, seen approximately in the same orientation. Site *AS*1 is very similar to RNase A: $O^{\delta 1}$ of the Asp121 carboxylate group is hydrogen bonded to the $N^{\varepsilon 2}$ of His119 and to a water molecule, which in turn is linked to the amide N atom of Asn67, while the other O atom $O^{\delta 2}$ is hydrogen bonded to the amide group of Lys66. In *AS*2, residues 567 to 569 are displaced toward His619 and the side chain of Gln69 would give short contacts with the histidine in a t conformation. However, there is space for a water molecule (Wat 665 in Fig. 12) which bridges the side chain of Gln569 to Sul125. In addition the side chain of Asp621 is rotated of about 20° (Table 6) toward the NH groups of Lys566 and Asn567 to which it is directly hydrogen bonded, with the elimination of the water molecule bridging $O^{\delta 1}$ to the amide group of Asn67 in *AS*1. $O^{\delta 1}$ of Asp621 is also hydrogen bonded to the $N^{\varepsilon 2}$ of Gln569.

As already found for the semisynthetic ribonuclease by Martin *et al.* (1987), $N^{\delta 1}$ of histidine in

Table 6. *Side-chain torsion angles* (°) *and hydrogen bonds* (Å) *for His*119 *and Asp*121

d_1 is the distance between $O^{\delta 1}$ of Asp121 and $N^{\varepsilon 2}$ of His119 in the t conformation; d_2 and d_3 are the distances between the closest O atom of the sulfate and $N^{\delta 1}$ of His119 in the t and g^- conformation, respectively.

	His119(t)		His119(g^-)		Asp121				
	χ^1	χ^2	χ^1	χ^2	χ^1	χ^2	d_1	d_2	d_3
RNase A (5RSA)	153	80	–	–	−157	55	2.74	2.36	–
RNase A (3RN3)	149	106	−76	−55	−151	73	2.61	2.53	3.15
Semisynthetic RNase (1SRN)	–	–	−51	−69	−165	59	–	–	2.93
BS-RNase (this work) *S*1	156	78	−66	−57	−156	54	2.76	2.66	2.82
*S*2	–	–	−65	−64	−178	73	–	–	2.96

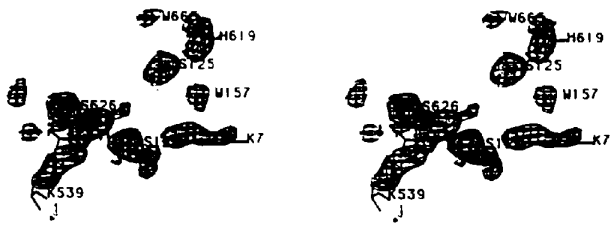

Fig. 11. Stereo drawing of the electron density from an omit ($|F_o| - |F_c|$)exp($i\alpha_c$) map (see *Sulfate anions*) around the sulfate anions close to *AS*2, with the final model shown as thick lines. The map was contoured at the 2 and 7σ levels.

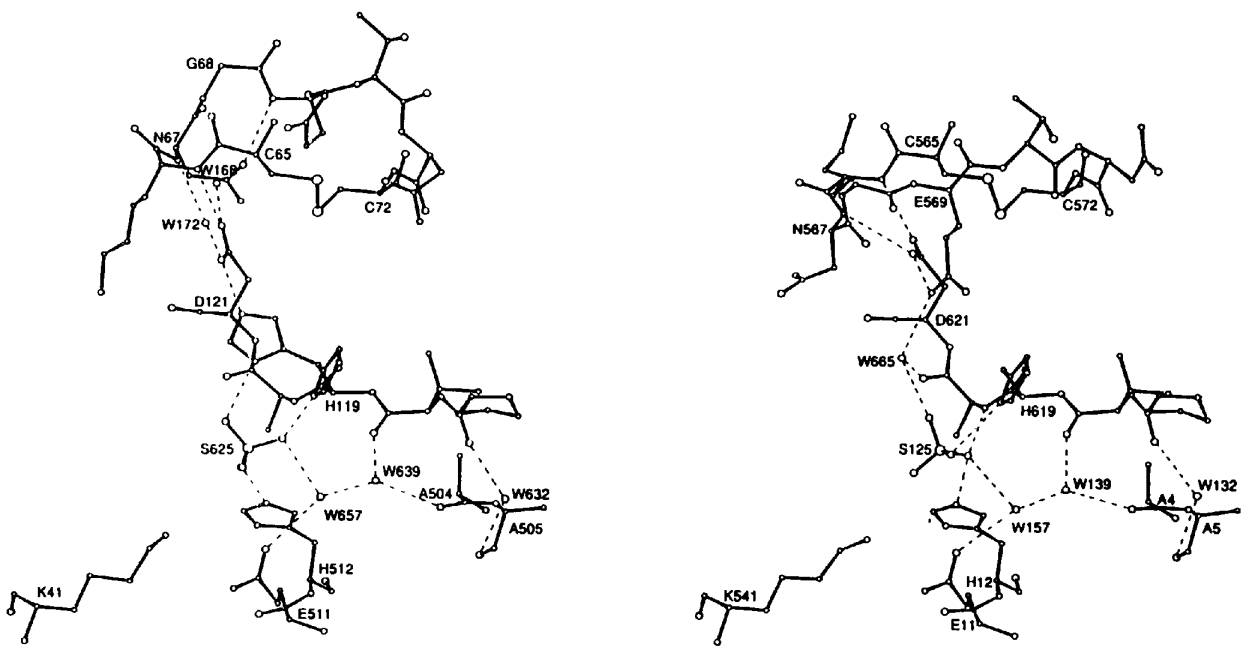

Fig. 12. View of the active sites *AS*1 (left) and *AS*2 (right). Hydrogen-bond interactions are represented by broken lines.

the g^- conformation is hydrogen bonded to an O atom of the sulfate anion in the active site. In our case, a further contribution to the stabilization of the alternative conformation is provided by the hydrogen bond between $N^{\varepsilon 2}$ and a water molecule interacting with the carbonyl group of Gly38 of a screw-related molecule.

Sulfate anions

The recognition pattern between ribonuclease and its natural substrate RNA includes specific interactions between the phosphate groups of the substrate and charged side chains of the enzyme. Besides the principal phosphate-binding site P_1 located at the active site of the enzyme, several studies on RNase A have produced evidence for the existence of additional phosphate-binding subsites called P_0 and P_2 (de Llorens, Arùs, Parés & Cuchillo, 1989). On the other hand, the sulfate group closely mimics the phosphate group and its binding sites are of interest for mapping interaction sites of the substrate with the enzyme. In particular, it has been shown (Piccoli *et al.*, 1988) that the binding of cytidine 3′-phosphate to the seminal enzyme exhibits mixed types of cooperativity which can be explained on the basis of a model involving at least three binding subsites.

Crystals of seminal ribonuclease, a protein significantly more basic than the pancreatic molecule, were grown from concentrated ammonium sulfate solutions, thus sulfate anions are likely to be found specifically bound to the exposed surface of the protein. Indeed, six outstanding peaks on the difference electron-density map, very well related in pairs by the molecular symmetry operation, were modelled as sulfate anions. Fig. 11 shows a stereoview of the difference Fourier map, contoured at the level of 2 and 7σ, in the region of the three sulfates near *AS*2: for these calculations, the three sulfate anions, the side chains of Lys7, Lys539, Lys541, His619 and the water molecules interacting with them were removed from the coordinate list and 60 cycles of refinement were performed. Similar calculations were performed for the three sulfates near *AS*1 and the resulting map (not shown) was also very similar.

As expected, a pair of maxima (Sul125 and Sul625) was located at the site P_1 in a position equivalent to that found in RNase A. The hydrogen-bonding interactions with the histidine residues and the water molecule in the active sites were discussed in the previous section. No direct hydrogen bond is formed with N^{ζ} of Lys41, which is 3.7 and 4.1 Å distant from the closest O atom of the sulfate group in the two active sites, respectively. However, the side chain of this lysine residue is well defined only up to the C^{δ} atom and the terminal-amino group has a definitely weaker density. In the refined position this group also contacts the side chains of Gln11 and Asn44.

A second pair of maxima (Sul127 and Sul627) was located between Lys7 and Lys39, each anion being hydrogen bonded to N^{ζ} of the two lysine residues, and not far from a third lysine residue (Lys613) of a screw-related molecule. This position is in agreement with the postulated subsite P_2 close to Lys7 in RNase A (de Llorens *et al.*, 1989). In our structure the distance between Sul127 and Sul125 is 7.8 Å, a value very close to the expected distance between two consecutive phosphate anions along a ribonucleotide chain. The third pair (Sul126 and Sul626), located in a niche above Pro42, is hydrogen bonded to N^{ζ} of Lys39 and is also hydrogen bonded to the amide N atom of Ala4 at the beginning of the helix *H*1 of a screw-related molecule, therefore receiving further stabilization from the helical dipole moment (Ptitsyn, 1969; Hol, van Duijnen & Berendsen, 1978). It is not clear how far the site is from the P_3 site, which according to de Llorens *et al.* (1989) is near Lys37 and Arg39 in RNase A. In the seminal enzyme these residues are replaced by Gln and Lys, respectively, and the sulfate group is indeed bound to Lys39, although it is on the distant side with respect to Gln37 and only 6.0 Å from Sul127.

Finally, a sulfate anion Sul128 was also fitted to a large density located at about 3 Å from the crystallographic diad axis in a cavity between two symmetry-related molecules. There are no positively charged groups of the protein within van der Waals distance of the sulfate; however, the guanidinium group of Arg580 is about 6 Å apart and the water molecule *W*690 (possibly an ammonium ion), placed on the diad axis, is hydrogen bonded to the O atoms of Sul128 and its symmetry-related mate. The sulfate O atoms are the recipients of additional hydrogen bonds from four residues of two different molecules. Like Sul126, this ion is located at the N terminus of the helix *H*2.

Bound water molecules

Of the numerous peaks observed in the difference electron-density map and initially assigned to water molecules, only 113 survived at the end of the refinement. Each water molecule was within hydrogen-bonding distance either from donor or acceptor atoms of the protein or from another water molecule or sulfate anion. According to their prevalent interactions, 56 water molecules were assigned to *S*1 and 57 to *S*2. The histogram in Fig. 13 shows the distribution of water thermal parameters. They are clustered about the r.m.s. value of 27.8 $Å^2$ and only a few molecules have a *B* factor outside the range 10–45 $Å^2$.

The non-crystallographic symmetry provides an internal check of the modelled solvent structure bound to the protein, at least for water molecules contacting only one protein molecule in regions which do not deviate significantly from the molecular symmetry. An inspection of these contacts reveals that about 70 molecules in the independent unit fulfil these conditions and 50 of those are remarkably well related in pairs by the pseudo-twofold symmetry. Indeed, when the appropriate (*T*1/*B*2 to *T*2/*B*1) transformation is applied, the r.m.s. deviation for these 25 pairs is 0.44 Å, which is reduced to 0.35 Å for a subset of 18 pairs, with a maximum deviation of 0.52 Å.

Also of interest is the comparison of the bound water molecules between the seminal and pancreatic enzymes, within the limits caused by the differences in crystal packing and primary structure of the two proteins, and by the fact that the seminal enzyme, as a dimer, offers a smaller surface exposed to the solvent. In view of the marked difference in the crystallization medium of the two proteins and bearing in mind all the restrictions previously mentioned, it is interesting that 18 out of the 25 water molecules, which occur in pairs in the seminal enzyme, are less than 1.0 Å from water molecules located in the pancreatic structure, and 10 are within 0.5 Å. Most of these water molecules correspond to high and well shaped maxima in the difference electron-density map.

Several water molecules strengthen the interchain *T*1/*B*2 and *T*2/*B*1 interactions (intrachain in the pancreatic enzyme). *W*132 and *W*139, which connect, *via* the carbonyl O atoms, Ala5 to Pro117 and Ala4 to Phe118, respectively (see Table 4), are also well preserved in RNase A (on superposition their positions differ by 0.20 and 0.37 Å, respectively). *W*139 is also linked to another conserved molecule *W*157, which is located in the active site and is hydrogen bonded to Sul125 and to the side chain of Glu11 (Fig. 12). In addition *W*135, bonded to the side chain of Glu11, and *W*148, interacting with Met35 and Lys39, are hydrogen bonded to the sulfate anion Sul127. The positions of *W*135 and *W*148 in *S*2 and *S*1 are well related by the molecular symmetry, but their positions bear only a rough relation to water molecules in the pancreatic enzyme. In the last case, however, the sulfate anion 127 is absent and Lys39 is replaced by an arginine residue.

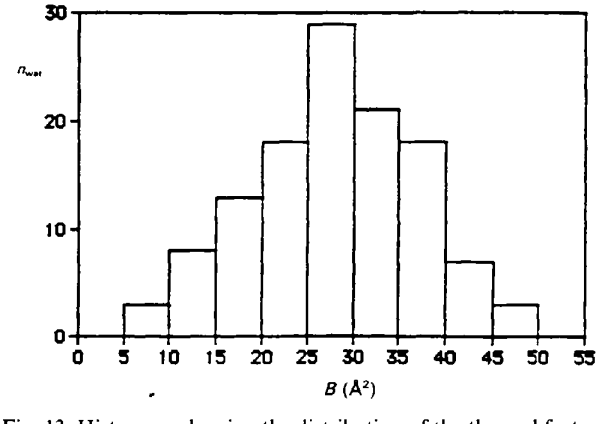

Fig. 13. Histogram showing the distribution of the thermal factors for water molecules.

An outstanding example of a strictly conservative hydration pattern in the exposed region of the N-terminal segment is provided by the water molecules *W*131 and *W*133. The carboxylate group of Glu2 is salt bridged to Arg10, forming two hydrogen bonds with $N^{\eta 2}$ and N^{ϵ} of the guanidinium group. A chain of hydrogen bonds is also formed, which starts from one of the carboxyl O atoms of Glu2 and includes *W*131, *W*133 and the carbonyl O atom of Ala6, which also participates in the α-helix hydrogen bond with the NH group of Arg10. This hydrogen-bonding network, located on the exposed side of the *H*1 helix, is extremely well preserved in RNase A and in the seminal enzyme, despite the large difference in the crystallization medium, and its stability is probably linked to the enhanced hydrogen-bonding energy associated with the charged groups. At the end of the same helix, a cluster formed by four water molecules *W*134, *W*136, *W*137 and *W*152 bridges the carbonyl O atom of Met13 to the NH and O^{γ} groups of Ser15 and to the carboxylate group of Glu9, although *W*152 is definitely in a different position in the two subunits. *W*134 and *W*136 have a good correspondence in the pancreatic molecule.

In the body *B*, the five water molecules *W*138, *W*141, *W*143, *W*144 and *W*158 are preserved in both enzymes and the high reproducibility of their positions (0.2–0.5 Å) highlights the importance of this cluster in maintaining the structure of the backbone region 95–100 and its position relative to the α-helical region 23–27 (Fig. 14). The hydration pattern of the helix *H*3 is also very similar in the two subunits and in the pancreatic enzyme: Wat150 bridges the carboxylate groups of Glu49 and Asp53, while a cluster of two water molecules *W*142 and *W*151 joins the carboxyl O atom of Asp53 to the side chain of Gln60.

Packing

The combination of space-group symmetry $P22_12_1$ with the molecular diad axis, approximately parallel to **c**, gives the crystal packing a pseudo *I*222 symmetry. With exact *I*222 symmetry, several short intermolecular contacts would occur between molecules translated along **b**, and all the major distortions, observed for the molecules in the solid state, can be

related to these contacts. The small tilt (ψ in Table 3) of the molecular axis and the different conformations adopted by the exposed loop 65–72 in *S*1 and *S*2 cooperate efficiently to release these contacts. Even the small translational component τ of the symmetry operation, which relates the two *T*/*B* functional domains, helps to this end. However, it cannot be stated whether this is an effect of the crystal packing or it reflects an intrinsic asymmetry of the molecule.

Specific packing interactions also occur across the crystallographic twofold axis. The dimers contact each other through the β-strand 94–110 of one chain and the same β-strand of the second chain, forming a hydrogen bond between the carbonyl group of Gln101 and the NH group of Glu103 (CO···NH, 2.77 Å). In this region several water molecules (Wat170, Wat171 and Wat177) mediate the interactions between polar groups of the two dimers. These packing interactions do not perturb the structure at the level of the backbone atoms, as judged by the close similarity of the two chains and of each chain with RNase A.

Concluding remarks

Considering the various aspects of the structure, bovine seminal ribonuclease can be regarded as the dimeric form of the pancreatic enzyme. The high degree of similarity of the primary structure and of functional properties of the two enzymes have a correspondence in the substantial similarity of their three-dimensional structure. However, from a topological aspect, the quaternary structure of BS-RNase is not created by a simple assembly of two pancreatic-like monomers but it is also characterized by the interchange of their N-terminal segments. This phenomenon is not completely new for RNase A either, as indeed it has been already shown that this enzyme aggregates under special conditions to give dimers, which also have the *T* segments interchanged (Crestfield, Stein & Moore, 1963; Fruchter & Crestfield, 1965).

From this point of view, the seminal enzyme can be considered to have evolved from the pancreatic molecule with the further constraints of the interchain disulfide bridges, which stabilize the dimer while allowing the interchange of the *T* segments. The axes of the *H*2 helices of the two chains form an angle of about 40°, allowing good interactions between the side chains of Ile28 and Met29 across the molecular diad axis. It should be mentioned that in RNase A residue 28 is Asn and is exposed to the solvent. Both the observed relative orientation of the helices and the conformation of the interchain disulfides are not usual in proteins (Richardson, 1981). As judged qualitatively from the model (Fig. 2), the surface of the sixteen-membered ring on the top side of the helices is largely exposed to the solvent and this is likely to be one of the reasons for the high reactivity of the interchain disulfides toward reducing agents (Parente, Merrifield, Geraci & D'Alessio, 1985).

By selective reduction of these disulfides a monomeric species can be obtained which is fully active (Piccoli & D'Alessio, 1984). This result implies that the monomer has to recover the same relative spatial relationship that the *T*/*B* segments have in RNase A and, consequently, a somewhat similar folding of the hinge peptide. Therefore, it should also be possible to model a dimeric species without interchanging the *T* segments, so that each active site is formed by residues from a single chain. Indeed, such a dimer was shown to be present in solution as a minor component by Piccoli *et al.* (1992), although it is not incorporated in the crystals at any appreciable level. All these findings clearly indicate that seminal ribonuclease has the unique property of reconstituting two distinct types of fully functional active sites by a different folding of the polypeptide chain.

Basically, the active sites of BS-RNase, as found in the crystal state, are very similar to that of RNase A, even though they are formed by residues belonging to different chains. The differences between the two sites in the dimer can be related to crystal packing, which probably causes the large change observed in the conformation of the loop 65–72; it is also not

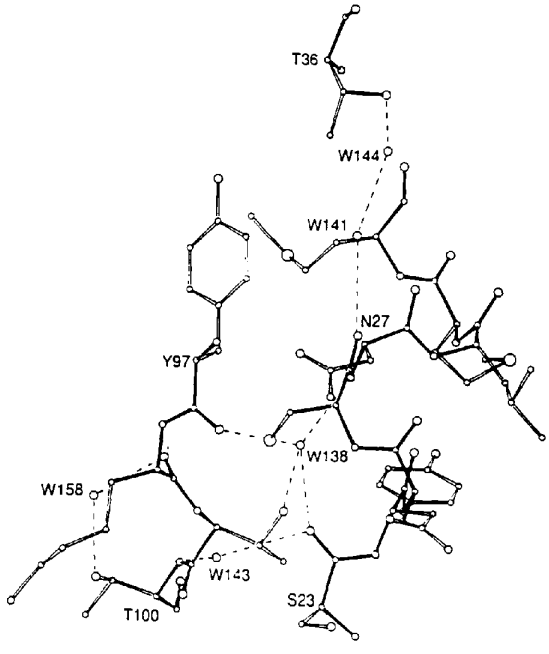

Fig. 14. A group of highly conserved water molecules for *S*1. Broken lines indicate hydrogen bonds involving water molecules. The same pattern is also observed for *S*2 and for RNase A.

clear to what extent details in this region might be obscured by the chain heterogeneity resulting from a partial deamidation of Asn67. However, we believe that the features observed are reliable and they provide further evidence of the high mobility of His119 in contrast to the behaviour of the other catalytically important histidine (His12), which is firmly bound to the protein matrix as in RNase A.

The strong correlation of the hydration shell between the two subunits of the seminal enzyme and between the seminal and pancreatic enzymes, while indicating the general reliability of the determined water positions, also underlines the role that the invariant water molecules play in the stabilization of the tertiary structure of the proteins.

Finally, the good correspondence between the position of the sulfate ions found in this structure and the phosphate-binding sites, postulated by Cuchillo and coworkers (de Llorens *et al.*, 1989) on the basis of a number of experimental data for RNase A, gives indirect evidence for a substantial similarity of interaction of the two proteins with RNA.

The authors warmly acknowledge Dr A. Wlodawer at the Macromolecular Structure Laboratory of the National Cancer Institute in Frederick (Maryland, USA) who kindly made available the X-ray diffraction apparatus used in this work, Dr G. D'Alessio for continuous stimulating discussions and a gift of the purified enzyme, Drs A. Wlodawer and G. Nemethy for a critical reading of the manuscript, and Mr G. Sorrentino for technical assistance. This work was financially supported by the Italian CNR and MURST.

References

AGARWAL, R. C. (1978). *Acta Cryst.* A**34**, 791–809.

ASHIDA, T., TSUNOGAE, Y., TANAKA, I. & YAMANE, T. (1987). *Acta Cryst.* B**43**, 212–218.

BLACKBURN, P. & MOORE, S. (1982). *The Enzymes*, edited by P. D. BOYER, 3rd ed., pp. 317–443. New York: Academic Press.

BORKAKOTI, N., MOSS, D. S. & PALMER, R. A. (1983). *Acta Cryst.* B**38**, 2210–2217.

BRÜNGER, A. T., KARPLUS, M. & PETSKO, G. A. (1989). *Acta Cryst.* A**45**, 50–61.

BRÜNGER, A. T., KURIYAN, K. & KARPLUS, M. (1987). *Science*, **235**, 458–460.

CAMPBELL, R. L. & PETSKO, G. A. (1987). *Biochemistry*, **26**, 8579–8584.

CAPASSO, S., GIORDANO, F., MATTIA, C. A., MAZZARELLA, L. & ZAGARI, A. (1983). *Biopolymers*, **22**, 327–332.

CAPASSO, S., GIORDANO, F., MAZZARELLA, L. & RIPAMONTI, A. (1972). *J. Mol. Biol.* **64**, 311–312.

CAPASSO, S., MAZZARELLA, L. & ZAGARI, A. (1991). *Pept. Res.* **4**, 234–238.

CRESTFIELD, A. M., STEIN, W. H. & MOORE, S. (1963). *J. Biol. Chem.* **238**, 2421–2428.

D'ALESSIO, G., DI DONATO, A., PARENTE, A. & PICCOLI, R. (1991). *Trends Biochem. Sci.* **16**, 104–106.

DI DONATO, A. & D'ALESSIO, G. (1973). *Biochem. Biophys. Res. Commun.* **55**, 919–928.

DI DONATO, A. & D'ALESSIO, G. (1981). *Biochemistry*, **20**, 7232–7237.

FRUCHTER, R. G. & CRESTFIELD, A. M. (1965). *J. Biol. Chem.* **240**, 3875–3882.

HOL, W., VAN DUIJNEN, P. & BERENDSEN, H. (1978). *Nature (London)*, **273**, 443–446.

HOWARD, A. J., GILLILAND, G. L., FINZEL, B. C., POULOS, T. L., OLHENDORF, D. H. & SALEMME, F. R. (1987). *J. Appl. Cryst.* **20**, 383–387.

HOWLIN, B., MOSS, D. S. & HARRIS, G. W. (1989). *Acta Cryst.* A**45**, 851–861.

IUPAC–IUB COMMISSION ON BIOCHEMICAL NOMENCLATURE (1970). *J. Mol. Biol.* **52**, 1–17.

JONES, T. A. (1978). *J. Appl. Cryst.* **11**, 268–272.

JONES, T. A., ZOU, J. Y., COWAN, S. W. & KJELDGAARD, M. (1991). *Acta Cryst.* A**47**, 110–119.

LLORENS, R. DE, ARÚS, C., PARÉS, X. & CUCHILLO, C. M. (1989). *Protein Eng.* **2**, 417–429.

LUZZATI, V. (1952). *Acta Cryst.* **5**, 802–810.

MARTIN, P. D., DOSCHER, M. S. & BRIAN, F. P. E. (1987). *J. Biol. Chem.* **262**, 15930–15938.

MAZZARELLA, L., MATTIA, C. A., CAPASSO, S. & DI LORENZO, G. (1987). *Gazz. Chim. Ital.* **117**, 91–97.

NACHMAN, J., MILLER, M., GILLILAND, G. L., CARTY, R., PINCUS, M. & WLODAWER, A. (1990). *Biochemistry*, **29**, 928–937.

PARENTE, A., MERRIFIELD, B., GERACI, G. & D'ALESSIO, G. (1985). *Biochemistry*, **24**, 1098–1104.

PICCOLI, R. & D'ALESSIO, G. (1984). *J. Biol. Chem.* **259**, 693–695.

PICCOLI, R., DI DONATO, A. & D'ALESSIO, G. (1988). *Biochem. J.* **253**, 329–336.

PICCOLI, R., TAMBURRINI, M., PICCIALLI, G., DI DONATO, A., PARENTE, A. & D'ALESSIO, G. (1992). *Proc. Natl Acad. Sci. USA*, **89**, 1870–1874.

PONDER, J. W. & RICHARDS, F. M. (1987). *J. Mol. Biol.* **193**, 775–791.

PTITSYN, O. (1969). *J. Mol. Biol.* **42**, 501–510.

RAMAKRISHNAN, C. & RAMACHANDRAN, G. N. (1965). *Biophys. J.* **5**, 909–933.

RICHARDSON, J. S. (1981). *Adv. Protein Chem.* **34**, 167–339.

WILSON, A. J. C. (1949). *Acta Cryst.* **2**, 318–321.

WLODAWER, A. (1985). *Biological Macromolecules and Assemblies*, Vol. II, *Nucleic Acids and Interactive Proteins*, edited by F. JURNAK & A. MCPHERSON, pp. 395–439. New York: Wiley.

WLODAWER, A. & SJÖLIN, L. (1983). *Biochemistry*, **22**, 2720–2728.

WLODAWER, A., SVENSSON, L. A., SJÖLIN, L. & GILLILAND, G. L. (1988). *Biochemistry*, **27**, 2705–2717.